

Peculiarities of the superconducting gaps and the electron-boson interaction in $\text{TmNi}_2\text{B}_2\text{C}$ as seen by point-contact spectroscopy

Yu. G. Naidyuk, O. E. Kvitnitskaya, L. V. Tiutrina, I. K. Yanson*

B. Verkin Institute for Low Temperature Physics and Engineering,

National Academy of Sciences of Ukraine, 47 Lenin Ave., 61103, Kharkiv, Ukraine

G. Behr†, G. Fuchs, S.-L. Drechsler, K. Nenkov, and L. Schultz

Leibniz-Institut für Festkörper- und Werkstoffforschung Dresden e.V., Postfach 270116, D-01171 Dresden, Germany

(Dated: September 13, 2011)

Point-contact (PC) investigations on the title compound in the normal and superconducting (SC) state ($T_c \simeq 10.6$ K) are presented. The temperature dependence of the SC gap of $\text{TmNi}_2\text{B}_2\text{C}$ determined from Andreev-reflection (AR) spectra using the standard single-gap approximation (SGA) deviates from the BCS behavior in displaying a maximum at about $T_c/2$. A refined analysis within the two-gap approximation provides evidence for the presence of a second gap twice as large as the main gap (the first one), while the latter is close to that within the SGA. This way, $\text{TmNi}_2\text{B}_2\text{C}$ expands the number of nickel borocarbide superconductors which exhibit a clear multiband character. Additionally, for the first time "reentrant" features were found in the AR spectra for some PCs measured in a magnetic field. The PC spectroscopy of the electron-boson interaction in $\text{TmNi}_2\text{B}_2\text{C}$ in the normal state reveals a pronounced phonon maximum at 9.5 meV and a more smeared one around 15 meV, while at higher energies the PC spectra are almost featureless. Additionally, the most intense peak slightly above 3 meV observed in the PC spectra of $\text{TmNi}_2\text{B}_2\text{C}$ is presumably caused by crystalline-electric-field (CEF) excitations. The peak near 1 meV detected for some PC spectra is connected with a modification of the CEF probably due to boron or carbon vacancies, allowing to probe the local stoichiometry by PC spectroscopy.

PACS numbers: 73.40.Jn, 74.45.+c, 74.70.Dd

I. INTRODUCTION

Compared with the isomorphous nonmagnetic transition metal borocarbides $R\text{Ni}_2\text{B}_2\text{C}$ with $R=\text{Y, Lu, Sc, La, Th}$, the rare-earth nickel borocarbide $R\text{Ni}_2\text{B}_2\text{C}$ (here R is a rare-earth element) compounds with $R=\text{Dy, Ho, Er, and Tm}$ are of special interest due to two coexisting and competing ordered states in these systems: antiferromagnetic (AFM) and superconducting (SC), observed by electrical resistivity, specific heat, magnetization, neutron, etc. measurements (see Refs. ¹⁻⁴ and Refs. therein). The energy scales of these two states are of similar size, with the SC critical temperature T_c both larger (for $R=\text{Ho, Er, and Tm}$) and lower (for $R=\text{Dy}$) than the AFM Néel temperature T_N . The SC state here is most probably of the BCS type and mediated by the electron-phonon interaction. The magnetism in these rare-earth compounds is provided by their localized $4f$ rare-earth ion's moments which order at relatively high temperatures compared with their dipole-dipole interaction due to the indirect Ruderman-Kittel-Katsuya-Yosida (RKKY) interaction mediated by the itinerant electrons. Moreover, the crystal electric field (CEF) splits the degenerate $4f$ rare-earth ion states. Thus, CEF effects may influence the formation of the AFM and SC states. For a deepened

understanding of $R\text{Ni}_2\text{B}_2\text{C}$ compounds spectral information both on the electronic structure and on the bosonic collective excitations are of importance.

Point-contact (PC) spectroscopy⁵ is a unique tool to study simultaneously both the SC gap or order parameter and to provide spectral data as to normal state bosonic excitations (phonons, magnons, CEF excitations etc.) always present in these solids. Measuring the second derivative of the $I(V)$ curves for the PC's, information about the electron-phonon interaction function $\alpha^2F(\omega)$ ⁶ and analogously for other bosonic collective interactions in the normal state can be obtained. Also the behavior of the SC gap (i.e. of the order parameter in a more rigorous sense) in the SC state can be determined from the $dV/dI(V)$ curves using a now routine approach⁷.

In this paper we focus on PC measurements on a rather special member of the rare-earth nickel borocarbide family, $\text{TmNi}_2\text{B}_2\text{C}$, which becomes superconducting below 11 K. But only below $T_N \simeq 1.5$ K does an AFM ordering appear where transversely polarized spin-density waves with an incommensurate modulation of the magnetic moments sets in.¹⁻⁴ Thus $\text{TmNi}_2\text{B}_2\text{C}$ exhibits the largest difference between T_c and T_N in the whole $R\text{Ni}_2\text{B}_2\text{C}$ series, which points to a relatively weak magnetism which cannot destroy the superconductivity on large Fermi surface sheets (FSS's), but only weakens it, although sizably, strongly dependent on the purity of the single crystals and as well as on the field direction.¹⁻⁴ The superconductivity is nevertheless affected by the special *incommensurate* magnetic state and its fluctuation

*deceased

†deceased

above $T_N \simeq 1.5$ K, at least for somehow disordered samples (probably with respect to C-B local disorder). In this context the *short* periodicity of the incommensurate antiferromagnetic structure, ≈ 25 Å, as compared with the superconducting coherence length, $\xi \approx 125$ Å, is of interest⁸ and a further argument given there that magnetism and superconductivity affect each other. In the present paper we do not consider the very coexistence of magnetism and superconductivity because this is already outside the range of our experimental setup ($T > 1.6$ K). For the temperature range above T_N and at least for low external magnetic fields one may also expect to detect remnants of the multiple-gap features well-known for non-magnetic borocarbides.^{9–12} A clear hint for such a multiple-gap behavior is given by experimentally observed positive curvature pronounced here for the upper critical field applied \parallel to the *ab*-plane. Due to the large magnetization for $H \parallel$ to the *c*-axis, H_{c2} is most strongly suppressed and its positive curvature as well.¹³

To the best of our knowledge, no PC data concerning $\text{TmNi}_2\text{B}_2\text{C}$, are available, except our recent preliminary results.^{14,15} On the contrary, there are several papers devoted to investigation of other members of the nickel borocarbide family (see Refs.^{14–16} and Refs. therein), where the SC gap as well as the electron-phonon spectral function were studied. The peculiar non-monotonic temperature dependence of the upper critical field $H_{c2}(T) \parallel$ to the *c*-axis observed frequently¹⁷ has been attributed to Pauli paramagnetic effects¹⁸. All this makes investigations of the missing $\text{TmNi}_2\text{B}_2\text{C}$ by PC spectroscopy desirable in order to get a complete picture. Here we restrict ourselves to a study of the paramagnetic phase above $T_N \simeq 1.5$ K.

II. EXPERIMENTAL DETAILS

$\text{TmNi}_2\text{B}_2\text{C}$ single crystals were grown by the float-zone technique with optical heating.¹⁹ For homogenization and in order to minimize the amount of possible disorder on the boron and carbon sites, the crystals were wrapped into tantalum foil and subjected to a heat treatment at 1000° C for 72 h and subsequently at 500° C for 72 h under purified argon atmosphere. The residual resistance ratio [RRR = $\rho(300\text{ K})/\rho(11\text{ K})$] of the investigated crystal significantly increased by this heat treatment: from RRR=14 before heating to RRR=28 after it. The high perfection of the single crystals is confirmed by the small width (about 0.45 deg) of neutron diffraction peaks obtained for (103) Bragg reflection. The investigated single crystal had a resistivity of $\rho(11\text{ K}) = 1.7\ \mu\Omega\text{ cm}$ in the normal state. Its SC transition temperature amounts $T_c = 10.6$ K, determined from the midpoint value of the SC transition.

The PC spectra have been measured mainly along the *c* direction by a standard "needle-anvil" method,⁵ touching a cleaved $\text{TmNi}_2\text{B}_2\text{C}$ surface with a sharpened thin Cu wire. A number of PC spectra has been measured

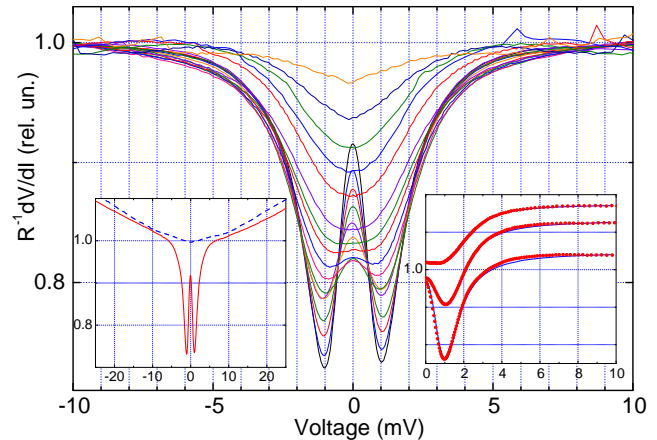


FIG. 1: (Color online) Normalized to the normal state and symmetrized dV/dI curves of a $\text{TmNi}_2\text{B}_2\text{C}$ -Cu contact ($R = 5.7\ \Omega$) established approximately in the *c* direction at temperatures from the bottom to the top: 1.6 K, 2 K, 2.5 K ... and further with 0.5 K step until 9.5 K (upper curve). Left inset: Example of a raw dV/dI curve at 1.6 K (solid curve) and 10 K (dashed curve) extended to the higher biases. Right inset: Some selected normalized and symmetrized dV/dI for the same PC (points) at $T=1.6, 3.5$ and 6 K (from the bottom to the top) along with calculated theoretical (according to the theory⁷) curves (thin lines).

perpendicular to the *c* direction, but we have found no qualitative difference between them and the PC spectra along the *c* direction. The reason might be that the cleaved surface was quite irregular and rough, therefore the crystallographic direction in PC is not well defined and the PC spectra are expected to be averaged over a large angle.

The differential resistance $dV/dI(V)$ and the second derivatives $d^2V/dI^2(V)$ were recorded through sweeping the *dc* current I on which a small *ac* current i was superimposed. The alternating voltage $V_1 \propto dV/dI(V)$ as well as its second harmonic $V_2 \propto d^2V/dI^2(V)$ have been recorded using the standard phase sensitive lock-in technique. It is well known that the first derivative $dV/dI(V) = R(V)$ of the $I(V)$ curve between a normal metal and a superconductor, the so-called Andreev-reflection (AR) spectrum, reflects the SC gap.⁷ The second derivative of the $I(V)$ curve of the type $R^{-1}dR/dV = R^{-2}d^2V/dI^2$ is directly proportional to the electron-boson spectral function according to the PC spectroscopy theory (see Ref.⁵, chapter 3 and Ref.⁶). This derivative can be readily obtained: simply by dividing the measured V_2 by V_1^2 , i.e., $R^{-1}dR/dV \propto V_2/V_1^2$.

III. PC SPECTROSCOPY OF THE SC ENERGY GAP

To obtain a spectroscopic insight into the SC energy gap as well as into the spectral function of the electron-

boson interaction, the contact size d should be smaller than the inelastic electron mean-free path. To avoid a variation of the SC gap on the scale of the PC size, also the contact diameter d should be less than the coherence length ξ , which is in $\text{TmNi}_2\text{B}_2\text{C}$ between 11 and 15 nm.^{8,17,20} The elastic electronic mean-free path in $\text{TmNi}_2\text{B}_2\text{C}$ is estimated as about $l \simeq 20$ nm, using typical for the nickel borocarbides $\rho l \simeq 3.6 \times 10^{-12} \Omega \text{ cm}^2$ (see Ref.²¹) and our residual resistivity $\rho_0 \simeq 1.7 \mu\Omega \text{ cm}$. According to Wexler's formula²² $R_{\text{PC}} \simeq 16\rho l/3\pi d^2 + \rho/2d$, (here we neglected contribution to the second term from the resistivity of a normal metal (needle) and suppose geometrically equal parts occupied by each metal in the case of heterocontact), the PC diameter d can be estimated from their resistance R_{PC} and ρl . Using a typical R_{PC} between 1 Ω and 10 Ω , one estimates a d value between 30 nm and 10 nm. Thus, the necessary condition of the smallness of the PC size compared to l and ξ may be fulfilled for the investigated PCs. Even more importantly from the experimental or practical point of view is the observation of characteristic AR features in the $dV/dI(V)$ spectra in the SC state along with the phonon structure in $d^2V/dI^2(V)$ in the normal state, which can be used as criteria for a spectroscopic (ballistic or diffusive⁵) regime in PC.

We succeeded in obtaining high-quality dV/dI PC characteristics as shown in Fig. 1, which demonstrates clear AR features – deep minima around $V \simeq \pm\Delta/e$ at $T \ll T_c$, here Δ is the SC gap, and the absence of any other irregularities like spikes, humps, etc. For most PCs, the structure (minimum) which characterizes the SC state disappears at about 10 K, slightly below the mentioned bulk $T_c \simeq 10.6 \pm 0.05$ K. The experimental dV/dI curves were fitted according to the well-known modified BTK theory (see Ref.⁵, section 3.7) within the single gap approximation (SGA). In the inset of Fig. 1, as an example, the calculated dV/dI along with the measured ones are shown at several temperatures. From the fitting of experimental dV/dI at different temperatures, the temperature dependencies of the SC gap Δ , the so-called Dynes or broadening parameter Γ ,²³ the barrier strength Z , and the scaling factor S have been determined (see Fig. 2 and Appendix).

As shown in Fig. 2, Γ and Z are nearly constant, excluding the region close to T_c . However, in this region above 6 K the double minimum structure in dV/dI is washed out and the self-action computer procedure gives more room for the fitting parameters by approaching T_c . The most interesting feature is the temperature dependence of the gap $\Delta(T)$. As shown in Fig. 2, $\Delta(T)$ deviates from the BCS-type behavior, reaching a maximum not at $T \rightarrow 0$, but at about $T \simeq 5 \text{ K} \simeq T_c/2$. The majority of investigated PCs reveals a similar behavior for the extracted Δ . Moreover, the minima positions in dV/dI which at low temperatures should be close to the Δ value also display maximum (see Fig. 2) directly supporting the obtained specific $\Delta(T)$ behavior in this temperature region. The upper critical field $H_{c2}(T)$ measured for fields

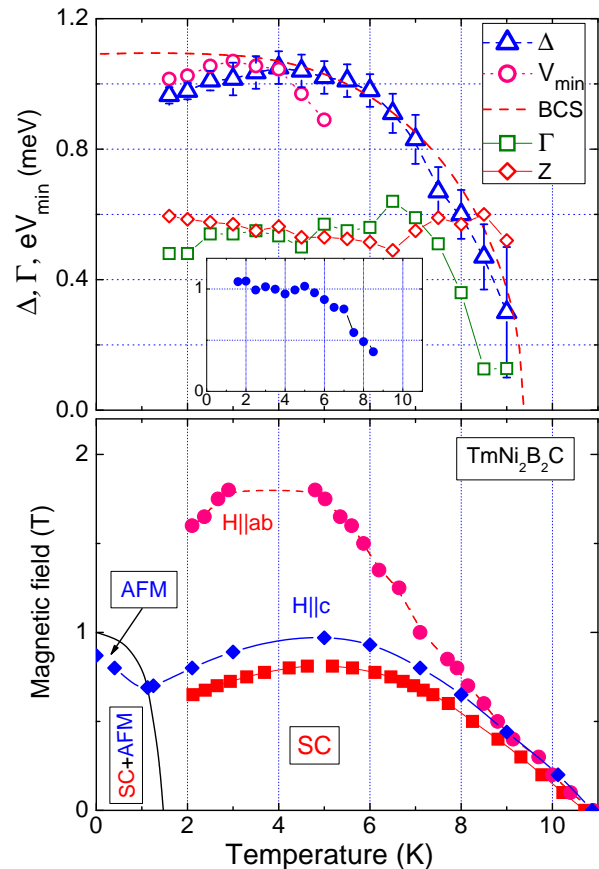


FIG. 2: (Color online) Upper panel: Temperature dependencies of the fitting parameters (within the SGA) for the PC spectra from Fig. 1: the SC gap Δ (triangles), the broadening parameter Γ (squares), the barrier parameter Z (diamonds) as well as the scaling factor S in the inset. The minimum position in dV/dI is shown by circles. Bottom panel: Phase diagram for both superconductivity and AFM spin-density wave order of $\text{TmNi}_2\text{B}_2\text{C}$ using data from⁸ along with our critical magnetic field data along the c -axis (squares) and ab -plane (circles).

along the c direction and within the ab plane behaves similarly (see Fig. 2), that is, it has a maximum. This broad maximum is closely related to the reentrant behavior found in the temperature dependence of both the bulk resistivity (see inset of Fig. 5) and of the magnetic susceptibility of $\text{TmNi}_2\text{B}_2\text{C}$ in magnetic field. Obviously, the recovery of the normal state at low temperature in the presence of a sufficiently high applied magnetic field is responsible for the anomalous decrease of $H_{c2}(T)$ at low temperatures. This $H_{c2}(T)$ anomaly might support our finding. In fact, since in the clean limit one has in the orbital approximation (ignoring a possible Pauli limiting behavior mentioned above¹⁸) $H_{c2}(T) \propto \Delta^2(T)$, the anomalous decrease of the upper critical field is more pronounced in the gap itself.

The gap distribution for the selected 14 contacts with pronounced AR minima along with the characteristic ratio $2\Delta/k_B T_c$ are shown in Fig. 3. The SC gap value Δ_0 (in

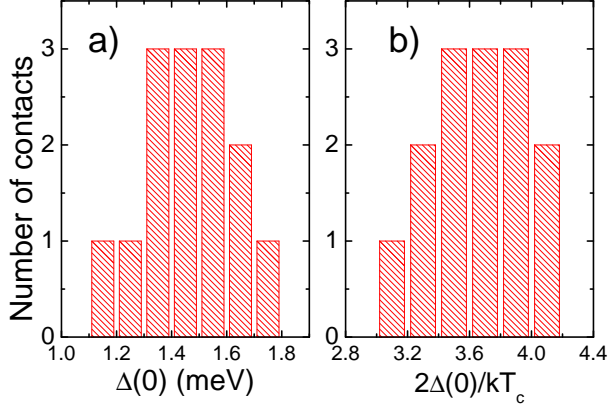


FIG. 3: (Color online) Distribution of the single SC gap $\Delta(0)$ extrapolated by the BCS curve to $T=0$ K (left panel) and the characteristic ratio $2\Delta(0)/k_B T_c$ (right panel) for the measured contacts. Notice the different shapes of both histograms reflect the different T_c values of various probed PCs.

the SGA extrapolated by the BCS dependence to $T=0$) results in a somewhat wide range $\Delta_0 = 1.1 - 1.7$ meV, which reveals a characteristic ratio $2\Delta/k_B T_c$ between 3 and 4.2,⁵² here T_c is the temperature where the AR features for the corresponding contact vanish, in other words, the local T_c . It varies between 9 and 10 K. Then the mean $2\Delta_0/k_B T_c$ exceeds the BCS weak coupling value 3.52, which points quite generally to a strongly coupled SC state. Alternatively, it might also reflect simply the local gap anisotropy on a given FSS. In order to explain the nearly isotropic H_{c2} in $\text{DyNi}_2\text{B}_2\text{C}$ ^{24,25} (see, e.g., Fig. 6 in Ref.²⁶), a somewhat anisotropic electron-phonon interaction and also a corresponding gap anisotropy must be assumed to compensate the *different* anisotropy of the Fermi velocities of the calculated cushion FSS, which would also affect H_{c2} . A similar enhanced gap ratio is also characteristic for other $R\text{Ni}_2\text{B}_2\text{C}$ compounds^{14,15} measured by AR spectroscopy. The gap distribution in $\text{TmNi}_2\text{B}_2\text{C}$ might be connected both with the anisotropy and the multiband superconductivity, as suggested by the analysis of the PC data for the nonmagnetic $\text{LuNi}_2\text{B}_2\text{C}$,^{10,27} $\text{YNi}_2\text{B}_2\text{C}$,¹¹ and the AFM $\text{ErNi}_2\text{B}_2\text{C}$ ²⁸ superconductors, or for the well-known two-gap superconductor MgB_2 .²⁹ On the other hand, existing tunneling spectroscopy data for $\text{TmNi}_2\text{B}_2\text{C}$ ³⁰ read: $\Delta_0 = 1.45$ meV and $2\Delta_0/k_B T_c \simeq 3.1$ with error bars of $\pm 15\%$. Additionally, they did not show a remarkable anisotropy and exhibit a BCS-like weak-coupling temperature dependence of the gap in the whole temperature range, even in the AFM region below 1.2 K.

Analyzing in more details our data and the SGA fitting parameters, it turned out that: 1) usually a quite large $\Gamma \geq \Delta/2$ is needed to fit the dV/dI curves, 2) the scaling factor S (see Appendix) varies considerably (see, e.g., Fig. 2), 3) there is a wide distribution of the gaps. The large Γ might point to a spatial (or directional) gap

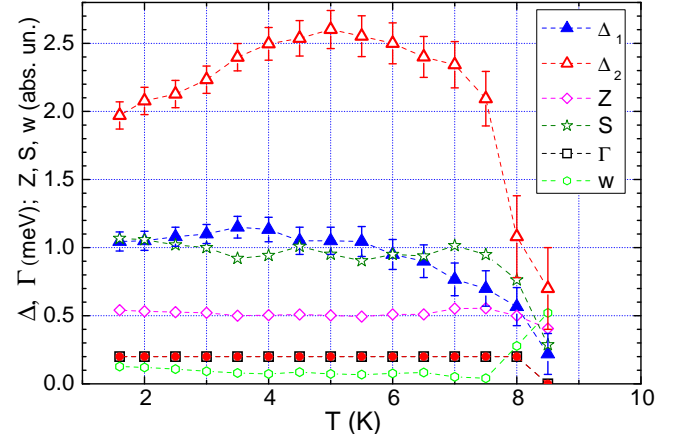


FIG. 4: (Color online) Temperature dependencies of the fitting parameters in the two-gap approximation (TGA): small (closed triangles) and large (open triangles) the SC gaps $\Delta_{1,2}$, the broadening parameters $\Gamma_1 = \Gamma_2 = 0.2$ (squares), the barrier parameter Z (diamonds), the scaling factor S (stars), and the contribution (weight factor) w to the dV/dI curve of the large gap (open circles). Error bars for the gaps show the difference between the presented gap values and the gaps calculated supposing $\Gamma_2 \simeq 2\Gamma_1$ (see also footnote Ref. #54).

distribution due to anisotropy or the multiband character of the SC state, a picture which is now widely accepted in the borocarbide community. Therefore, supposing a multiband SC state we have also carried out a two-gap fit.⁵³ In general, this fit is similar to the one-gap fit shown in Fig. 1(right inset), only the two-gap fit is a bit better in the 4–6 mV range for the dV/dI curves at the lowest temperatures. The results are shown in Fig. 4. First of all we note that 1) Γ is constant and more than two times smaller than that of our SGA fit⁵⁴ and 2) the scaling factor is close to 1 and varies moderately, except the region close to T_c , where the fit gives more freedom for fitting parameters due to a temperature broadening and smearing of a double-minimum structure of dV/dI . These two observations suggest that the obtained results of our two-gap fit are physically reasonable. As it is seen from Fig. 4, the small gap exhibits a more or less similar behavior as the gap obtained in the SGA fit, while the second gap is two times larger, but its contribution to the spectra is about 10%, once again excluding the region close to T_c . Thus we found plausible arguments for the presence of a second SC gap in $\text{TmNi}_2\text{B}_2\text{C}$. To clarify its nature, detailed directional PC investigations are desirable.

In the end of this section we would like to mention that except $\text{YbNi}_2\text{B}_2\text{C}$ with heavy-fermion like properties, at first glance the electronic structure as predicted by the first electronic structure calculations based on the local density approximation (LDA) is hardly affected by the rare-earth component directly.³¹ In particular, all these compounds exhibit a special FSS, called in the case of $R=\text{Lu, Y, Ho}$ and Dy as “cushion”³² or “pillow”³³ which

is formed only by Ni 3d states, i.e., without an admixture of rare-earth 5d derived states. The latter mediate the RKKY exchange coupling of the magnetic moments of the 4f electrons to some of the conduction electrons whose superconductivity is then strongly affected by the presence of the localized rare-earth magnetic moments. On the contrary, the superconductivity on the "cushion" FSS is almost perfectly protected against local magnetic fields caused by the exchange interaction between its conduction electrons and the 4f-moments. However, recent band structure calculations for TmNi₂B₂C show explicitly that some FSS has somewhat changed their shape. In particular, the "cushion" has not been detected.³⁴ By symmetry an analogous Ni-3d derived FSS free of an admixture with Tm 5d states should nevertheless exist. Since its exact shape has not been resolved yet, we denote it, for the sake of simplicity, as "pseudo-cushion" (pc)-FSS. On these grounds a similar local SC gap of ≈ 1 meV can be expected for that pc-FSS in TmNi₂B₂C, too. The PC data for the smaller gap reported above (which is less sensitive to the vicinity of magnetism) provide strong support for such an assignment in the title compound, too. The larger second gap reported here, too, with a stronger sensitivity to the vicinity of magnetism corresponds to the major FSS in nonmagnetic borocarbides, which in the present case is somewhat affected by the fluctuations of this AFM state occurring below 1.6 K.

A. "Reentrant" features for dV/dI characteristics in an external magnetic field

Let us turn to the measurements of dV/dI in an external magnetic field. By studying the obtained curves one can distinguish two types of dV/dI behavior. One of them is shown in the upper panel of Fig. 5. Here the external magnetic field does not substantially change the position of the dV/dI minima (reflecting the SC gap) up to fields of about 1 T. The magnetic field reduces the intensity of the whole dV/dI minimum and its influence looks like a smearing of the AR minima. A qualitatively similar behavior is observed for most of PCs based on the title compound and on many other superconductors, including nickel borocarbides^{11,12,16,35} as well as simple SC metals, e.g., Nb³⁶. In the meantime the dV/dI for some studied PCs have demonstrated a quite different behavior,⁵⁵ similar to that shown in Fig. 5(b). Here, the double-minimum structure undergoes significant modifications in a magnetic field. Below 0.6 T the dV/dI curves behave like in the previous case, but at higher field they transform into another structure with a plateau-like maximum at zero bias, so that the zero-bias resistance reaches its normal-state value at 0.7 T and then this normal-state region spreads out to higher voltages by further field increase until all dV/dI curves transform into a parabolic-like normal-state behavior.

This structure of dV/dI in Fig. 5(b) looks similar to

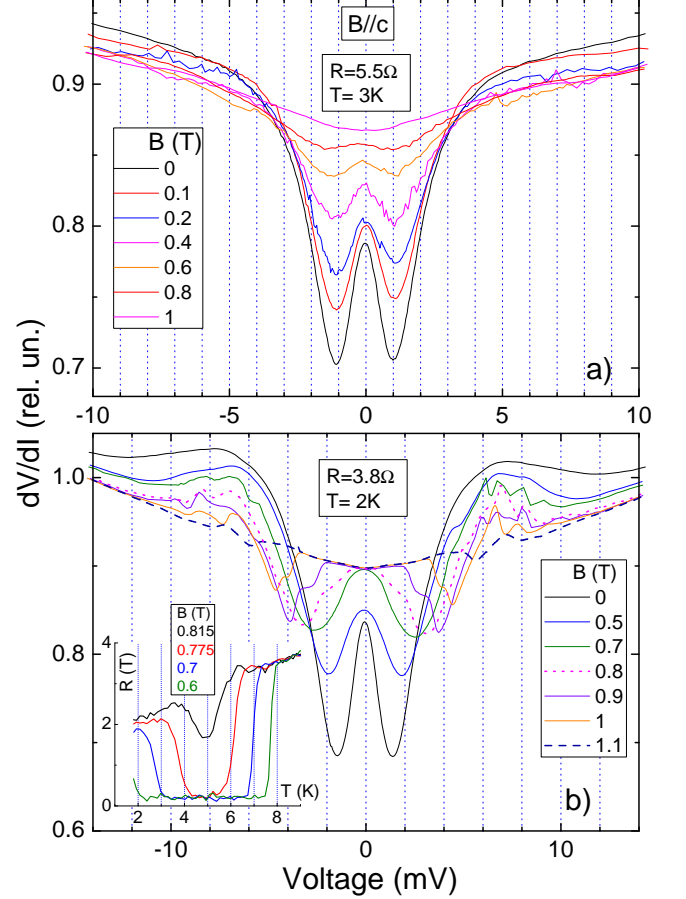


FIG. 5: (Color online) a) Raw dV/dI curves of contact from Fig. 1 (after the temperature measurements) measured at $T=3$ K in magnetic field. b) Raw dV/dI curves of another TmNi₂B₂C-Cu contact measured at $T=2$ K in a magnetic field. Note the transformation of the zero-bias maximum into a plateau-like structure above 0.7 T. Inset: reentrant features in the resistance of a TmNi₂B₂C single crystal in an external magnetic field $\mathbf{B} \parallel \mathbf{c}$.

reentrant behavior found in the temperature dependence of the bulk resistivity of TmNi₂B₂C in the external magnetic field⁵⁶, where the normal state is restored at 2 K in a field above 0.7 T (see inset in Fig. 5b). This behavior of the bulk resistivity, i.e., the recovering of the normal state at low temperature under a magnetic field, may be connected with some kind of magnetic ordering induced by the external magnetic field. The temperature increase (e.g., above 2 K at 7 T, see inset in Fig. 5b) destroys this state and recovers the SC state. We assume that in our case the applied voltage plays a role similar to the temperature, namely, a relaxation of strongly nonequilibrium electron distribution function in a PC under an applied voltage⁶ can produce nonequilibrium phonons with an effective temperature $\leq eV/4$ ³⁷. Therefore in our case applied voltage increase recovers the SC state (SC features in dV/dI) in the field above 7 T at 2 K.

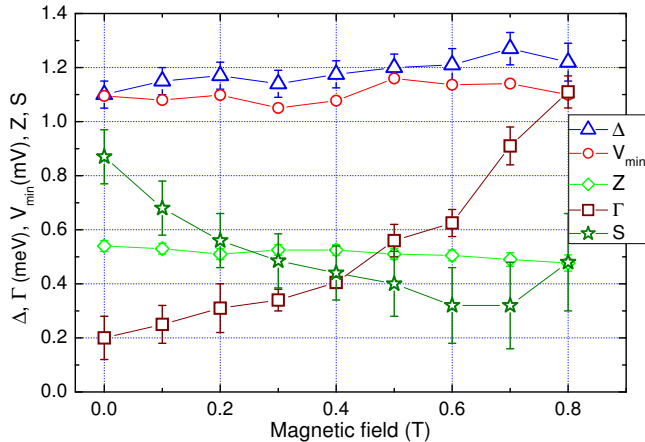


FIG. 6: (Color online) Magnetic field dependencies of the fitting parameters within the SGA taken at $T=3\text{K}$: the SC gap Δ (triangles), the broadening parameter Γ (squares), the barrier parameter Z (diamonds), the scaling factor S (stars), as well as the minimum position in dV/dI (circles) extracted from the PC spectra in Fig. 5(a).

This qualitatively different behavior observed in both types of dV/dI characteristics is consistent with the observation that reentrant behavior of $\rho(T)$ in a magnetic field is not found for all $\text{TmNi}_2\text{B}_2\text{C}$ single crystals.³⁸

We have also recovered the magnetic field dependence of the SC gap and of the other fitting parameters again in the SGA. The results are shown in Fig. 6 using the spectra from Fig. 5(a). It turned out that the effective single gap is almost magnetic field *independent*, strictly speaking, it exhibits even a slight increase. This observation is in accord with the minima position in dV/dI . However, this unusual, absolutely counterintuitive and striking behavior (never observed for any superconductor to the best of our knowledge) might be ascribed to an unresolved anisotropic multigap scenario. In fact, provided the PC reflects also some (*ab*)-geometry, a gap contribution from non-cushion FSS's with a much higher upper critical field H_{c2} than the depicted highest field of 1 T might readily resolve the puzzle.

Γ steeply increases in an external magnetic field as it has been found for many other type-II superconductors,^{5,36} while in type-I superconductors Γ is almost field independent.³⁹ The increase of Γ is usually connected with a shortening of the bosonic (Cooper pairs) life-time due to the pair-breaking effect of an external magnetic field.⁴⁰ The scaling parameter S decreases with the magnetic field. This can be understood as a shrinkage of the SC volume in the PC region, probably due to vortex penetration. However, the determination of the SC gap and other parameters from AR spectra in a magnetic field using the standard BTK approach with the introduction of the SC density of states smearing due to life-time effects²³ only is, in principle, a simplified approach. As mentioned in Ref.⁴¹, the SC density

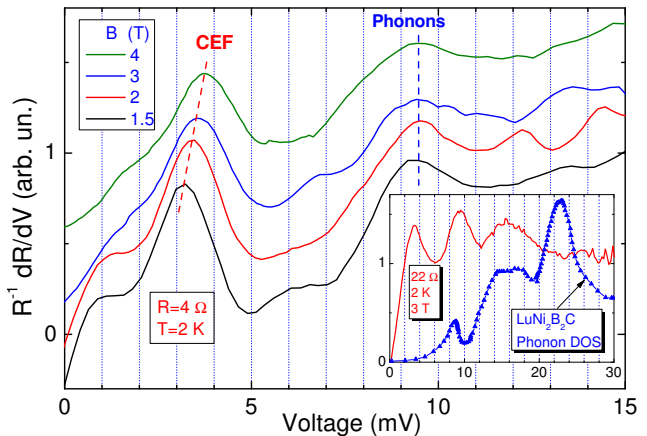


FIG. 7: (Color online) $R^{-1}dR/dV \propto d^2V/dI^2$ curves measured at 2 K in a magnetic field for the 3.8Ω PC from Fig. 5(b). The inset shows the PC spectrum of another 22Ω PC with sharper phonon maxima along with the phonon DOS for $\text{LuNi}_2\text{B}_2\text{C}$ (symbols).

of states in the mixed state varies in space, i. e., becomes *nonuniform*. This special situation requires an appropriate theoretical description (not available at present) for the density of states to compute realistic AR spectra. Moreover, the local SC density of states in PC will depend on the position of the pinned vortex with respect to the PC core. Therefore the obtained effective parameters of the homogeneous model and their magnetic field dependence extracted from AR spectra measured in an external magnetic field above the lower critical field H_{c1} should be interpreted with some caution.

IV. PC SPECTROSCOPY OF BOSONIC EXCITATIONS IN THE NORMAL STATE

Now we consider the measured PC electron bosonic interaction spectra ($R^{-1}dR/dV = R^{-2}d^2V/dI^2$ curves) of $\text{TmNi}_2\text{B}_2\text{C}$ -Cu PCs. These spectra show clear maxima at about 3 mV and 9.5 mV (see Fig. 7) and a more smeared maximum at 15 mV (see inset in Fig. 7 and the following figures). The maxima at about 9.5 mV and 15 mV were not affected by magnetic field and correspond well to the low-energy maxima in the neutron phonon density of states of the nonmagnetic isostructural compound $\text{LuNi}_2\text{B}_2\text{C}$ ⁴² (see Fig. 7, inset), only the high-energy part of the obtained PC spectra remains almost featureless. The displayed in the PC spectra phonon features are similar to those observed in other nickel borocarbide compounds.^{11,14,16,27,43,44} Thus, the observed peaks reflect the $\text{TmNi}_2\text{B}_2\text{C}$ phonons excited by the inelastic scattering of electrons (energized by eV-bias). Unfortunately, even for the PC with a relatively large resistance (see Fig. 7, inset) for which the conditions for the ballistic (spectroscopic) regime is fulfilled

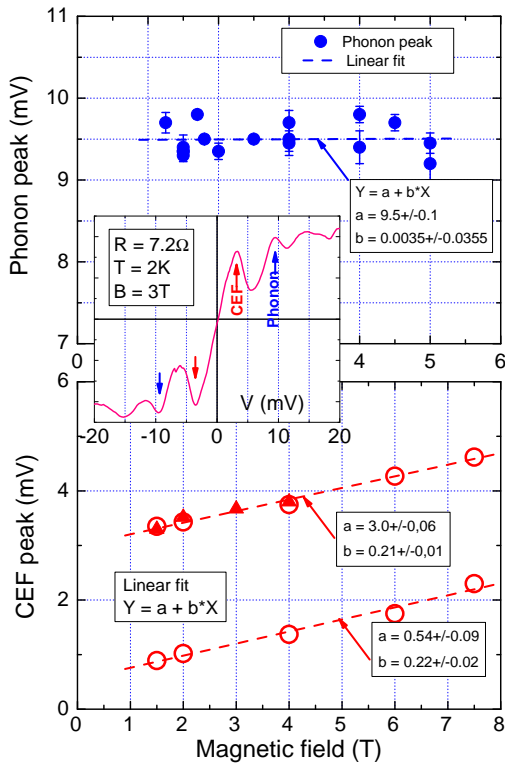


FIG. 8: (Color online) Upper panel: Position of the phonon peak on $R^{-1}dR/dV \propto d^2V/dI^2$ PC spectrum (shown in inset) for several $\text{TmNi}_2\text{B}_2\text{C}$ -Cu contacts versus magnetic field. Bottom panel: position of CEF peak(s) from Fig. 7 (triangles) and Fig. 9 (circles). Dashed lines demonstrate linear fit of the data. Inset shows the typical PC spectrum with mentioned peaks marked by the arrows.

with a larger probability, so far we could not resolve the phonon features above 20 mV, contrary to the case of $\text{HoNi}_2\text{B}_2\text{C}$.¹⁴ One of the reasons might be that the PC spectrum of $\text{TmNi}_2\text{B}_2\text{C}$ contains a dominant 3-mV peak, which is connected with CEF excitations as is shown below. Thus, excitations of Tm ions to the first CEF level by eV-energized electrons followed by subsequent scattering on 9.5-mV and 15-mV phonons will lead to a shortening of the inelastic electron mean free path and to deviations from the ballistic (spectroscopic) regime in our PC with further increasing of bias eV. This blocks energy-resolved spectroscopy at higher energies.

Next we will consider the mentioned low-energy peak near 3 mV, where the peak positions are marked by the tilted dashed line in Fig. 7. It can be assigned with the first excited CEF transition in $\text{TmNi}_2\text{B}_2\text{C}$ according to Ref.⁴⁵. As shown in Fig. 8, a magnetic field shifts this maximum to higher energies whereas the maximum at about 9.5 mV remains fixed. This confirms phononic origin of the 9.5-mV maximum. The other CEF transitions at the higher energies mentioned in Ref.⁴⁵ could not be resolved in the PC spectra, probably due to their lower intensity and the mentioned deviation from the spectro-

scopic regime with the bias increase. Thus, this low-lying first CEF excitation seems to play a dominant role in the transport properties of $\text{TmNi}_2\text{B}_2\text{C}$. The presence of such low-energy excitations in $\text{TmNi}_2\text{B}_2\text{C}$ can be anticipated from the nonsaturated resistivity in this compound by lowering temperature with pronounced slope of $\rho(T)$ until T_c (see Fig. 5(b), inset).

We have also occasionally measured PC spectra with an additional peak at low energy near 1 mV (see Fig. 9). A magnetic field shifts this peak as well as the second peak at about 3 mV (see Fig. 8, bottom panel) to the higher energies, whereas the positions of the phonon maxima near 10 and 17 mV are stable. The 3-mV peak looks like the CEF peak on the previous spectra. The 1-mV peak persists up to the highest fields available in our experiment (7.5 T) exceeding the H_{c2} in the ab and c directions by a factor of four or two, respectively. Such a behavior in a magnetic field excludes any residual superconductivity in our PCs as the origin of this peak⁵⁷. The appearance of this 1 mV peak may testify to the nonstoichiometry of $\text{TmNi}_2\text{B}_2\text{C}$ in the PC core. In contrast to $R=\text{Ho}$, Er compounds, here in the region of C and/or B vacancies or disordered C and B sites the original magnetic Tm-ion ground state doublet splits into two singlet states (see Ref.⁴, page 768). If so, then on the one hand the PC spectroscopy enables us to distinguish the "fine structures" in the CEF schema of $\text{TmNi}_2\text{B}_2\text{C}$, while on the other hand it allows us to control the local stoichiometry. Another possibility is that $\text{TmNi}_2\text{B}_2\text{C}$ exhibits a quadrupolar ordered phase below $T_Q=13.5\text{ K}$ ⁴⁶. The consequence of this would be that the quadrupolar ordering lowers the CEF symmetry, resulting in the mentioned ground-state splitting. In this context we note that a weak peak at about of 1 meV has been observed in the inelastic neutron spectra of $\text{Tm}_{0.05}\text{Y}_{0.95}\text{Ni}_2\text{B}_2\text{C}$.⁴⁷ It was ascribed by the authors to a transition derived from a splitted, originally two-fold degenerate Tm-ion ground-state. Thus, we also assume here a similar transition resulting from a modified CEF Tm-ion ground state, either due to nonstoichiometry (vacancies) or due to a quadrupolar ordered phase. To finally elucidate the nature of these peaks, more detailed directional measurements in higher magnetic field with samples of well-defined stoichiometry are required as well.

V. CONCLUSION

We have carried out investigations of the SC gap and of the electron-bosonic interaction spectra in $\text{TmNi}_2\text{B}_2\text{C}$ by means of AR and PC spectroscopy, respectively. The SC gap in $\text{TmNi}_2\text{B}_2\text{C}$ is found to deviate considerably from the usual BCS-type behavior in showing a broad maximum at $T^* \simeq T_c/2$. An improved two-band analysis of our data also shows the presence of a second SC gap being about two times larger than the former, which remains close to the small "first" gap observed. The smaller gap

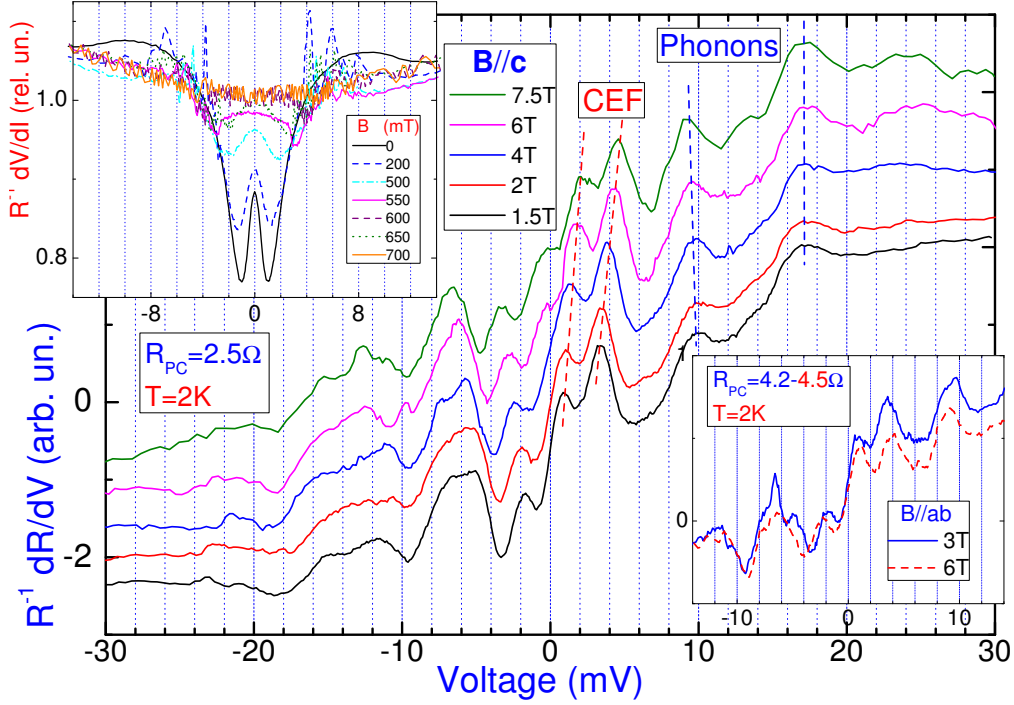


FIG. 9: (Color online) PC spectrum $R^{-1}dR/dV$ of TmNi₂B₂C-Cu PC for two bias polarity with additional 1 mV peak vs magnetic field. Left inset: dV/dI for the PC from the main panel at low fields, which also demonstrates “reentrant” features above 500 mT. Right inset: PC spectrum for another PC at two fields showing a similar low-energy 1-mV peak structure.

has been assigned to a FSS which has a similar orbital structure and a gap value as the “cushion” FSS found in other nickel-based 1221 borocarbide compounds. This not-yet-resolved FSS for TmNi₂B₂C is almost protected from the exchange interaction with the magnetic moments of the rare-earth ions. The observed second larger gap is only a bit smaller than the larger gap in nonmagnetic borocarbide superconductors. This way TmNi₂B₂C interpolates between “cushion”-FSS-dominated almost single-band superconductors DyNi₂B₂C and HoNi₂B₂C within the commensurate AFM state and the nonmagnetic borocarbide superconductors YNi₂B₂C, LuNi₂B₂C, and probably, also the ScNi₂B₂C compound which, however, is less well studied.

We succeeded to measure PC electron-bosonic interaction spectra of TmNi₂B₂C with distinct phonon features at 9.5 mV and 15 meV along with intense low-energy maxima of a nonphonon nature at about 3 meV and additionally at about 1 meV for some spectra. The 3-meV maximum is due to excitation of Tm ions on the upper (first) CEF level by eV-energized electrons. As to the 1-meV peak, it is likely connected with a modification of the CEF due to boron or carbon vacancies. This allows, in principle, for the PC spectroscopy to be regarded as a local probe to check the stoichiometry. Intense peaks of CEF excitations in PC spectra point to their significant contribution to the spectral function of the electron-boson interaction.

Acknowledgements

Two of us, Yu. G. N. and O. E. K., thank IFW-Dresden for hospitality and the Alexander von Humboldt Foundation for support. Support by Pakt für Forschung at the IFW-Dresden and the Deutsche Forschung Gemeinschaft as well as the National Academy of Sciences of the Ukraine are gratefully acknowledged. Discussions with H. Rosner, K.-H. Müller, and M. Schneider are kindly acknowledged.

Appendix

As a rule, the parameter Γ is used to describe the nonthermal smearing of the experimental dV/dI curves, namely, the broadening of the characteristic AR minima in dV/dI , while the original physical meaning of Γ in the Dynes model²³ as a finite lifetime of charge carriers due to inelastic scattering is usually not under consideration. This is because other effects contribute to the dV/dI broadening, e. g., as SC gaps distribution^{48,49} (via nonhomogeneity, surface, multiband, etc. effects) or gap anisotropy (see also §4.3.4 in Ref.⁵⁰).

Including Γ in the fit procedure leads not only to the smearing of the whole calculated dV/dI curve but also results in a reduced intensity of the whole AR (minima) structure. In this context we note, that for a high-quality

fit of dV/dI in full, not only the shape of dV/dI must be described, but also its absolute intensity must be correct. In the present paper we also address this point, namely, we considered the, so-called, scaling factor S , which is included to fit the intensity of calculated and experimental curves. For instance, $S=1$ means that the calculated curve fits the measured dV/dI also in absolute values. In the case of the ordinary superconductor with a large coherence length like Zn,³⁹ we succeeded in performing such a fit practically for all PCs. If $S < 1$, the measured dV/dI has a reduced intensity due to suppression of the AR signal or the opening of some non-AR channel in the PC conductivity. Thus, the authors of Ref.²⁸ assumed that $S < 1$ is realized when the Fermi surface is only partially gapped in the SC state. Of course, the more common explanation of non-SC regions in the PC or multicontact scenario, including PCs with suppressed superconductivity, cannot be ruled out as well. Thus, in Ref.⁴¹ a contribution to the conductance from the normal vortex cores in the superconductor was taken into account to describe a progressive suppression of the AR features in an external magnetic field.

It turned out that even a seemingly nonphysical situation with $S > 1$ can also take place. As a rule, large Γ values result in large $S > 1$. A more reasonable explanation would be the following: if the smearing of dV/dI is due to a variation (distribution) of SC gaps over the Fermi surface, then the description of this smearing by including Γ results in a reduced calculated dV/dI intensity and finally leads to a scaling parameter $S > 1$. Hence such a situation with $S > 1$ might point to a gap distribution or to a multiband scenario.

We should also mention that a contribution to the dV/dI minima may come from the Maxwell resistance,⁵ which cannot be ignored for materials with a high residual resistivity like, e.g., the heavy-fermion compounds.⁵¹ Since the residual resistivity in RNi_2B_2C compounds is above $1\mu\Omega\text{cm}$, then the Maxwell contribution to R_{PC} can exceed 1Ω for a PC with a diameter of 10 nm. The vanishing of the Maxwell resistance in the SC state can lead to a situation where the PC resistance (the conductance) can decrease (increase) more than 2 times, thus it exceeds the limit of the maximal AR signal.

-
- ¹ K.-H. Müller, V.N. Narozhnyi, Rep. Prog. Phys. **64**, 943 (2001).
 - ² K.-H. Müller, G. Fuchs, S.-L. Drechsler and V. N. Narozhnyi, in: "Magnetic and Superconducting Properties of Rare Earth Borocarbides of the Type RNi_2B_2C ", Handbook of Magnetic Materials, Ed. by K.H.J. Buschow (Elsevier, North-Holland, 2002), Vol. 14, pp. 199-305.
 - ³ K.-H. Müller, M. Schneider, G. Fuchs and S.-L. Drechsler, *Handbook on the Physics and Chemistry of Rare Earths*, ed. by Karl A. Gschneidner Jr., Jean-Claude Bünzli, and Vitalij K. Pecharsky, (North-Holland, Elsevier, 2008), Vol. 38, p.175.
 - ⁴ L. C. Gupta, Adv. in Physics, **55**, 691 (2006).
 - ⁵ Yu. G. Naidyuk and I. K. Yanson, *Point-Contact Spectroscopy*, Springer Series in Solid-State Sciences, (Springer Science+Business Media, Inc, 2005), Vol.145.
 - ⁶ I. O. Kulik, A. N. Omelyanchouk and R. I. Shekhter, Sov. J. Low Temp. Phys. **3**, 840 (1977) [Fiz. Nizk. Temp. **3**, 1543 (1977)].
 - ⁷ G. E. Blonder, M. Tinkham and T. M. Klapwijk, Phys. Rev. B **25**, 4515 (1982); A. V. Zaitsev, Sov. Phys. - JETP **59**, 1015 (1984); A. Plecenik, M. Grajcar, S. Benacka, P. Seidel, and A. Pfuch, Phys. Rev. B **49**, 10016 (1994).
 - ⁸ P. L. Gammel, D. Lopez, D. J. Bishop, M. R. Eskildsen, N. H. Andersen, K. Mortensen, I. R. Fisher, K. O. Cheon, and P. C. Canfield, J. Appl. Phys., **87**, 5544 (2000).
 - ⁹ S. V. Shulga, S.-L. Drechsler, G. Fuchs, K.-H. Müller, K. Winzer, M. Heinecke, and K. Krug, Phys. Rev. Lett. **80** 1730 (1998).
 - ¹⁰ N. L. Bobrov, S. I. Beloborod'ko, L. V. Tyutrina, V. N. Chernobay, I. K. Yanson, D. G. Naugle and K. D. D. Rathnayaka, Low Temp. Phys, **32**, 489 (2006) [Fiz. Nizk. Temp. **32**, 641 (2006)].
 - ¹¹ D. L. Bashlakov, Yu. G. Naidyuk, I. K. Yanson, G. Behr, S.-L. Drechsler, G. Fuchs, L. Schultz and D. Souptel, J. Low Temp. Phys., **147**, 335 (2007).
 - ¹² P. Raychaudhuri, G. Sheet, S. Mukhopadhyay and H. Takeya, Physica C **460-462**, 95 (2007).
 - ¹³ J. P. Brison, N. Luchier, A. Sulpice, H. Suderow, P. Martinez-Samper, S. Vieira, A. I. Buzdin, and P. C. Canfield, J. of Magn. Magn. Mater. **272-276**, 158 (2004).
 - ¹⁴ Yu. G. Naidyuk, D. L. Bashlakov, N. L. Bobrov, V. N. Chernobay, O. E. Kvitnitskaya, I. K. Yanson, G. Behr, S.-L. Drechsler, G. Fuchs, D. Souptel, D. G. Naugle, K. D. D. Rathnayaka, J. H. Ross Jr., Physica C, **460-462**, 107 (2007).
 - ¹⁵ Yu. G. Naidyuk, G. Behr, N. L. Bobrov, V. N. Chernobay, S.-L. Drechsler, G. Fuchs, O. E. Kvitnitskaya, D. G. Naugle, K. D. D. Rathnayaka and I. K. Yanson, J. of Phys.: Conf. Series, **150**, 052178 (2009).
 - ¹⁶ Yu. G. Naidyuk, O. E. Kvitnitskaya, I. K. Yanson, G. Fuchs, K. Nenkov, A. Wälte, G. Behr, D. Souptel, and S.-L. Drechsler, Phys. Rev. B **76**, 014520 (2007).
 - ¹⁷ B. K. Cho, M. Xu, P. C. Canfield, L. L. Miller, and D. C. Johnston, Phys. Rev. B **52**, 3676 (1995).
 - ¹⁸ L. DeBeer-Schmitt, M. R. Eskildsen, M. Ichioka, K. Machida, N. Jenkins, C. D. Dewhurst, A. B. Abrahamson, S. L. Bud'ko, and P. C. Canfield, Phys. Rev. Lett. **99**, 167001 (2007).
 - ¹⁹ D. Souptel, G. Behr, W. Löser, K. Nenkov, and G. Fuchs, J. of Crystal Growth, **275**, e91 (2005).
 - ²⁰ M. R. Eskildsen, K. Harada, P. L. Gammel, A. B. Abrahamson, N. H. Andersen, G. Ernst, A. P. Ramirez, D. J. Bishop, K. Mortensen, D. G. Naugle, K. D. D. Rathnayaka and P. C. Canfield, Nature, **393**, 242 (1998).
 - ²¹ A. K. Bhatnagar, K. D. D. Rathnayaka, D. G. Naugle, P. C. Canfield, Phys. Rev. B **56**, 437 (1997).
 - ²² A. Wexler, Proc. Phys. Soc. (London) **89**, 927 (1966).
 - ²³ R. C. Dynes, V. Narayanamurthy and J. P. Garno, Phys. Rev. Lett. **21**, 1509 (1978).

- ²⁴ Z. Q. Peng, K. Krug and K. Winzer, Phys. Rev. B **57**, 8123(R) (1998).
- ²⁵ C. V. Tomy, M. R. Lees, L. Afalfiz, G. Balakrishnan, and D. Paul, Phys. Rev. **52**, 9186 (1995).
- ²⁶ J. Jensen and P. Hedegård, Phys. Rev. B **76**, 094504 (2007).
- ²⁷ O. E. Kvitnitskaya, Yu. G. Naidyuk, I. K. Yanson, T. Niemeier, G. Fuchs, B. Holzapfel and L. Schultz, Supercond. Sci. Technol. **23** 115001 (2010).
- ²⁸ N. L. Bobrov, V. N. Chernobay, Yu. G. Naidyuk, L. V. Tyutrina, D. G. Naugle, K. D. D. Rathnayaka, S. L. Budko, P. C. Canfield and I. K. Yanson, Europhys. Lett., **83**, 37003 (2008).
- ²⁹ I. K. Yanson, Yu. G. Naidyuk, Fiz. Nizk. Temp. **69**, 355 (2004) [Low Temp. Phys. **69**, 261 (2004)].
- ³⁰ H. Suderow, P. Martinez-Samper, S. Vieira, N. Luchier, J. P. Brison, and P. C. Canfield, Phys. Rev. B **64**, 020503(R) (2001).
- ³¹ S.B. Dugdale, C. Utfeld, I. Wilkinson, J. Laverock, Zs. Major, M.A. Alam, and P. Canfield, Supercond. Sci. Technol. **22**, 01402 (2009).
- ³² B. Bergk, V. Petzold, H. Rosner, S.-L. Drechsler, M. Bartkowiak, O. Ignatchik, A. D. Bianchi, I. Sheikin, P. C. Canfield, and J. Wosnitzer, Phys. Rev. Lett. **100**, 257004 (2008).
- ³³ S.-L. Drechsler, H. Rosner, I. Opahle, and H. Eschrig, Physica C **408-410**, 104 (2004).
- ³⁴ H. Rosner *et al.* to be published.
- ³⁵ X. Lu, W. K. Park, S. Yeo, K.-H. Oh, S.-I. Lee, S. L. Budko, P. C. Canfield, and L. H. Greene, Phys. Rev. B **83**, 104519 (2011).
- ³⁶ Yu. G. Naidyuk, R. Häussler, and H. von Löhneysen, Physica B, **218**, 122 (1996).
- ³⁷ I. O.Kulik, I. K. Yanson, A. N. Omelyanchouk, Fiz. Nizk. Temp. **7** 263 (1981) [Sov. J. Low Temp. Phys. **7** 129 (1981)]
- ³⁸ C. Lamprecht, Diploma thesis "Untersuchung der magnetischen und supraleitenden Eigenschaften von RNi_2B_2C (R - Ho, Tm)", TU Dresden, Dresden (2007). Notably, the reentrant behavior sometimes reported in the literature is not observed for all single crystals. Moreover, the upper critical field can differ by a factor of 2, even for annealed samples. This points, in our opinion, to the large role of residual disorder.
- ³⁹ Yu. G. Naidyuk, H. v. Löhneysen, and I. K. Yanson, Phys. Rev. B **54**, 16077 (1996).
- ⁴⁰ M. Tinkham, Introduction to Superconductivity (McGraw-Hill, New-York, 1980).
- ⁴¹ Y. Miyoshi, Y. Bugoslavsky, and L. F. Cohen, Phys. Rev. B **72**, 012502 (2005).
- ⁴² F. Gompf, W. Reichardt, H. Schober, B. Renker, M. Buchgeister, Phys. Rev. B **55**, 9058 (1997).
- ⁴³ I. K. Yanson, V. V. Fisun, A. G. M. Jansen, P. Wyder, P. C. Canfield, B. K. Cho, C. V. Tomy, and D. McK. Paul, Phys. Rev. Lett. **78**, 935 (1997).
- ⁴⁴ I. K. Yanson, N. L. Bobrov, C. V. Tomy, and D. McK. Paul, Physica C **334**, 152 (2000).
- ⁴⁵ U. Gasser, P. Allenspach, F. Fauth, W. Henggeler, J. Mesot, A. Furrer, S. Rosenkranz, P. Vorderwisch, M. Buchgeister, Z. Phys. B **101**, 345 (1996).
- ⁴⁶ N. H. Andersen, J. Jensen, T. B. S. Jensen, M. v. Zimmermann, R. Pinholt, A. B. Abrahamsen, K. Nørgaard Toft, P. Hedegård, and P. C. Canfield, Phys. Rev. B **73**, 020504(R) (2006).
- ⁴⁷ M. Rotter, C. Sierks, M. Loewenhaupt, J. Freudenberger and H. Schober, in *Rare Earth Transition Metal Borocarbides (Nitrides): Superconducting, Magnetic and Normal State Properties* eds. K.H. Müller and V. Narozhnyi (Kluwer Academic, Dordrecht, 2001), Vol.14, p.137.
- ⁴⁸ P. Raychaudhuri, D. Jaiswal-Nagar, G. Sheet, S. Ramakrishnan, and H. Takeya, Phys. Rev. Lett. **93**, 156802 (2004).
- ⁴⁹ N. L. Bobrov, S. I. Beloborodko, L. V. Tyutrina, I. K. Yanson, D. G. Naugle, and K. D. D. Rathnayaka, Phys. Rev. B **71**, 014512 (2005).
- ⁵⁰ D. Daghero and R. S. Gonnelli, Supercond. Sci. Technol. **23**, 043001(2010).
- ⁵¹ K. Gloos, F. B. Anders, B. Buschinger, C. Geibel, K. Heuser, F. Jahrling, J. S. Kim, R. Klemens, R. Müller-Reisner, C. Schank, G. R. Stewart, J. Low Temp. Phys. **105**, 37 (1996).
- ⁵² We measured systematically dV/dI with AR minima position close to 1 mV (see, e.g., Fig.1), corresponding to $2\Delta_0/k_B T_c \simeq 3$, which may be connected with both anisotropy and/or a multiband scenario. See also the further section concerning two-gap calculations.
- ⁵³ The two-gap(band) approach is supported also by a recent three-dimensional study of the Fermi surface of $LuNi_2B_2C$ ³¹, where the contributions to the total density-of-states (DOS) at the Fermi energy from three bands equal to 0.24%, 22.64% and 77.1%, respectively, have been found. That is, basically only two bands contribute to the total DOS.
- ⁵⁴ At first glance it seems naturally to suppose a two times larger Γ_2 for the twice as large second gap. However, in this case the contribution of the second gap (or weight factor) w strongly varies at low temperature (about 4 times): it decreases from 0.32 to 0.09 with temperature rising from 1.6 K to 4 K. In our opinion there is no physical reason for such behavior.
- ⁵⁵ The PC spectrum for this contact is shown in Fig.7. It demonstrates clear CEF and phonon maxima, therefore it is unlikely that specific dV/dI behavior is connected with a regime in PC that is not spectral (e.g., thermal). In our case humps in dV/dI around 6 mV are likely connected with critical current or critical (Oersted) field effects.
- ⁵⁶ We note, that the reentrant behavior in the magnetic field is not observed for all single crystals (according to unpublished data in Ref.³⁸) and does not occur for very clean samples. Moreover, the critical field can differ by a factor up to 2 even for annealed samples, which can be connected with difficulties to control the stoichiometry and the appropriate site position for boron and carbon.
- ⁵⁷ On the contrary, the hump near 1 mV in dV/dI at 1.5 and 2 T in Fig. 7 is likely caused by residual superconductivity because this structure disappears at higher fields.